ANALYSIS OF BLADE DEFORMATION EFFECT ON ROTOR BVI NOISE PREDICTION

G. Bernardini,* S. Ianniello† and M. Gennaretti*

*University Roma Tre
Dept. of Mechanical and Industrial Engineering
Via della Vasca Navale 79 - 00146 Rome, Italy

† INSEAN
Via di Vallerano 139 - 00128 Rome, Italy

Abstract

The acoustic field generated by helicopter main rotors experiencing blade-vortex interaction (BVI) is examined. The prediction tool starts from an aerodynamic solver based on a boundary integral formulation for the velocity potential, that is suited for configurations where wake/blade impingement occurs. It is fully 3D, can be applied to blades with arbitrary shape and motion and performs the calculation of both wake shape and blade pressure field. Then, an aeroacoustic tool based on the Ffowcs Williams and Hawkings equation is applied to evaluate the noise generated. The numerical investigation examines the sensitivity of the BVI noise predicted on the blade deformation included in the analysis. For helicopter rotors in descent flight, where severe BVI occurs, the effects of blade deformations are examined both in terms of local acoustic signatures and in terms of noise radiation characteristics.

List of Symbols

c	Speed of sound
$\mathcal{C}$	Panel contour
G	Green function
$\mathbf{M}$	Mach number vector
$\mathbf{n}$	Unit normal on a surface
p	Pressure
p'	Acoustic pressure disturbance
$\mathbf{P}$	Compressive stress tensor
$\mathbf{r}$	Source-observer distance vector
$\mathcal{S}$	Contour surface
t	Observer time
$\mathbf{T}$	Lighthill tensor
$\mathbf{v}$	Velocity field
$\mathbf{x}$	Observer position
$\mathbf{y}$	Source position
θ	Time delay
ρ	Air density
τ	Source time
φ	Velocity potential
χ	Normal velocity on the blade
Subscript	
0	Undisturbed medium
B	Body
I	Incident field
L	Loading
n	Component along surface normal direction
r	Component along source-observer direction
S	Scattered field
T	Thickness
W	Wake
Superscript	
F	Far wake
N	Near wake
TE	Trailing edge

1. Introduction

In the last years, the study of the close interaction as well as the collision of a helicopter rotor blade with the wake vortices released by the other blades of the rotor has been one of the biggest challenges facing the rotorcraft researchers. This phenomenon is known as blade-vortex interaction (BVI) and tipically occurs during descent flight and maneuvers at moderate advance ratio of a helicopter. It produces impulsive changes in blade surface pressure distribution that are of particular importance in the blade regions interacting with the high-strength trailing tip vortices [1]. Because of these impulsive loads, BVI is one of the main external noise sources, and hence has a great impact on the environmental and public acceptance of helicopters. The availability of reliable tools for the prediction of BVI aeroacoustics is essential for new generation helicopter design, where reduction of noise level is of great interest.

The physics of the BVI is governed by the shape of the rotor wake and by its distance from the blades. Thus, for an accurate prediction of this phenomenon, a computational tool should include both a three-dimensional unsteady-flow aerodynamic solver capable to analyze the wake shape evolution and an aeroelastic solver evaluating blade deformations. Tipically, prediction tools developed to examine rotorcraft in BVI conditions are based on the use of different codes for the wake distortion analysis and for the computation of the pressure distribution on the blade (the latter frequently based on 2D airfoil aerodynamics). For instance, this is the case of the study presented in Ref. [2] for aeroacoustics purposes, where a vortex-lattice free-wake is combined with a blade element theory for section load prediction, along with a system of low- and high-resolution grids to ensure a detailed analysis of BVI. The combined use of a dual vortex free-wake code with a 2D aerodynamics code is applied in Ref. [3] for the aeroelastic and aeroacoustic analysis of rotors aimed to vibration and noise reduction. In Ref. [4] the aerodynamic analysis of rotors in BVI conditions consists of a three-step procedure. The results of an initial vortex-lattice free-wake analysis are coupled with a roll-up model that identifies the higher-intensity vortex structure to be considered as the interacting vortices in a pressure predictor code based on a 2D solver. In the works mentioned above the aerodynamic analysis follows a previous aeroelastic calculation that predicts the blade deformation.

The objective of this paper is to analyze the sensitivity of the BVI noise predicted by a computational tool on the blade deformation included in the analysis. Specifically, considering both undeformed and deformed rotor blades, the acoustic fields are evaluated through the application of the boundary integral formulation for the aerodynamic analysis of rotors in BVI conditions introduced in Ref. [5], followed by an aeroacoustic solver based on the Ffowcs Williams and Hawkings equation [6]. For helicopter rotors in descent flight, where severe BVI occurs, the effects of blade deformations are examined both in terms of local acoustic signatures and in terms of noise radiation characteristics. The aerodynamic solver applied in this work is outlined in Section 2, whereas the aeroacoustic formulation is briefly described in Section 3. The numerical investigation is presented in Section 4.

This work has been developed within the context of the European Union Integrated Project *Friendcopter* that is aimed to the environmental friendliness and public acceptance of helicopters, through reduction of noise emission, gas exhaust and cabin noise levels. In particular, it is part of the activity concerning the definition of procedures for noise abatement.

2. The BEM Aerodynamic Solver for BVI Prediction

The aerodynamic formulation applied in this work has been introduced in Ref. [5] as a development of the boundary integral formulation for the velocity potential presented in Ref. [7].

For unsteady, incompressible, quasi-potential flows (*i.e.*, potential everywhere except on the zero-thickness wake surface) around lifting bodies in arbitrary motion with respect to the undisturbed air, the formulation given in Ref. [7] shows that the velocity potential field, φ, may be represented by the following boundary integral form

$$\begin{aligned}\varphi(\mathbf{x},t) &= \int_{\mathcal{S}_B}\left(G\frac{\partial\varphi}{\partial n}-\varphi\frac{\partial G}{\partial n}\right)\mathrm{d}\mathcal{S}\\ &- \int_{\mathcal{S}_W}\Delta\varphi\,\frac{\partial G}{\partial n}\mathrm{d}\mathcal{S},\end{aligned}\tag{1}$$

where $\mathcal{S}_B$ and $\mathcal{S}_W$ are body and wake surfaces, respectively, and $G=-1/4\pi|\mathbf{y}-\mathbf{x}|$ is the unit-source solution of the 3D Laplace equation (thus, the potential field is generated by a distribution of sources and doublets over the body, with the additional contribution of a doublet distribution over the wake surface). The impermeability boundary condition on $\mathcal{S}_B$ yields $\partial\varphi/\partial n=\mathbf{v}_B\cdot\mathbf{n}$, with $\mathbf{v}_B$ denoting velocity of body points and $\mathbf{n}$ denoting outward unit normal. In addition, $\Delta\varphi$ is the potential jump across the wake surface that is given by the Kutta-Joukowski condition [9], followed by convection of the trailing edge potential discontinuity, *i.e.*,

$$\Delta\varphi(\mathbf{x}_W,t)=\Delta\varphi^{TE}(t-\theta_W),\tag{2}$$

with θ_W denoting the time taken by the wake material point, $\mathbf{x}_W$, to move from the trailing edge to its current position (see Ref. [7] for details).

Equation (1) is solved numerically by boundary elements, *i.e.*, by discretizing $\mathcal{S}_B$ and $\mathcal{S}_W$ in quadrilateral panels, assuming φ, $\partial\varphi/\partial n$ and $\Delta\varphi$ to be piecewise constant, and imposing that the equation be satisfied at the center of each body element (collocation method). For the analysis of configurations where BVI occurs, Eq. (1) must necessarily be solved following a free-wake procedure, *i.e.*, determining the shape of the wake as a part of the solution. This is achieved by a time-marching integration scheme in which the vertices of the wake panels are moved accordingly to the velocity field computed from the potential solution. However, the numerical formulation based on Eq. (1) shows instabilities when the wake panel vertices come too close to or impinge the body (*i.e.*, just in BVI conditions). These instabilities are of numerical nature because of the inaccuracy in evaluating the influence wake doublet coefficients when the wake panels approach body surface control points, but are induced also by the unrealistic modeling of the physical phenomenon. Indeed, for a realistic modeling of a close interaction between wake and body, the inclusion of a non-zero thickness wake is essential because of the fundamental role played by the vorticity spatial distribution in determining the local fluid flow around the impact region.

In order to overcome this problem, the formulation proposed in Ref. [5] uses the vortex-doublet equivalence for the description of the wake influence. This approach is inspired by observing that: (*i*) the instabilities arising in the numerical formulation during wake/body impingement would be eliminated by replacing wake panel doublet distributions with equivalent ring thick vortices (namely, Rankine vortices) and (*ii*) the use of thick vortices allows the inclusion of diffusivity and vortex-stretching effects for a more realistic modeling of the flow field (see Refs. [8], [10] and [11] for details on this issue). A thick vortex model induces a velocity field that is assumed to have a finite-value distribution within its core. Therefore, the vortex influence can be calculated without loss of accuracy even when body or wake control points approach it, and a regular potential field is mantained.

In order to recast the potential integral equation in such a fashion that the wake portion experiencing BVI be expressed in terms of thick vortices, in Ref. [5] it is observed that at a given time, the doublet distributions over the wake panels that are not in contact with the trailing edge (*far wake*, $\mathcal{S}_W^F$) are known from the previous time steps and are not influenced by the current (unknown) potential over the body. In addition, the doublet distributions over the wake panels in contact with the trailing edge (*near wake*, $\mathcal{S}_W^N$) are unknown since related to current potential discontinuity at the trailing-edge of the blade (through the Kutta-Joukowski condition [9]), but no BVI occurs in that wake region (see Fig. 1). Thus, the potential field is decomposed into an *incident* field, φ_I, generated by doublets over $\mathcal{S}_W^F$, and a *scattered* field, φ_S, generated by sources and doublets over $\mathcal{S}_B$ and doublets over $\mathcal{S}_W^N$. Note that, the scattered potential is discontinuous across $\mathcal{S}_W^N$, whereas the incident potential is discontinuous across $\mathcal{S}_W^F$. Hence, as demonstrated in Ref. [5], for $\varphi = \varphi_I + \varphi_S$ the scattered potential is given by

$$\begin{aligned}\varphi_S(\mathbf{x},t) &= \int_{\mathcal{S}_B}\left[G\,(\chi-\chi_I)-\varphi_S\frac{\partial G}{\partial n}\right]\mathrm{d}\mathcal{S} \\ &- \int_{\mathcal{S}_W^N}\Delta\varphi_S^{TE}(t-\theta_W)\,\frac{\partial G}{\partial n}\mathrm{d}\mathcal{S}, \qquad (3)\end{aligned}$$

where $\chi = \mathbf{v}_B\cdot\mathbf{n}$ and $\chi_I = \mathbf{v}_I\cdot\mathbf{n}$, with the velocity induced by the far wake, $\mathbf{v}_I$, obtained by

$$\begin{aligned}\mathbf{v}_I(\mathbf{x},t) &= \nabla_{\mathbf{x}}\varphi_I(\mathbf{x},t) \\ &= -\nabla_{\mathbf{x}}\int_{\mathcal{S}_W^F}\Delta\varphi_S^{TE}(t-\theta_W)\,\frac{\partial G}{\partial n}\mathrm{d}\mathcal{S}. \qquad (4)\end{aligned}$$

The incident potential influences the scattered one by the induced-velocity term, χ_I, and, in turn, the scattered potential influences the incident one by its trailing-edge discontinuity that is convected along the wake and yields the doublet distribution over the far wake.

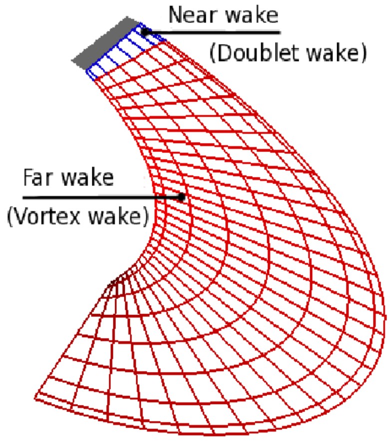

Figure 1. Wake decomposition.

Discretizing Eq. (4) by using N panels, $\mathcal{S}_{W_n}^F$, over the far wake and recalling the vortex-doublet equivalence, the incident velocity field is given by

$$\mathbf{v}_I(\mathbf{x},t)\approx -\sum_{n=1}^{N}\Delta\varphi_{S_n}^{TE}(t-\theta_W)\int_{\mathcal{C}_n}\nabla_{\mathbf{x}}\,G\times\mathrm{d}\mathbf{y} \qquad (5)$$

where $\mathcal{C}_n = \partial\mathcal{S}_{W_n}^F$. This equation represents the velocity field given by the Biot-Savart law applied to the vortices having the shape of the panel contours and intensity $\Delta\varphi_{S_n}^{TE}(t-\theta_{W\,n})$ (see Fig. 1). This field is equivalent and replace the one that would be given by the gradient of the doublet distributions that would appear in the discretized form of Eq. (4). Equation (5) is applied both to evaluate the term χ_I appearing in the equation for the scattered potential, and to determine the contribution of the incident velocity field to the wake distorsion in the free-wake analysis.

The final step of the formulation presented in Ref. [5] is to assure a stable and regular solution (even in BVI conditions) by introducing in Eq. (5) a thick vortex model, for which a finite distribution of the induced velocity within the vortex core is assumed. The dimension of the vortex core is obtained by an approximated evaluation of diffusivity and vortex-stretching effects, for a more realistic modeling of the flow field.

Once the potential field is known, the Bernoulli theorem yields the pressure distribution that in turn is used as input to the aeroacoustic solver to predict the BVI-induced noise. Note that, in this formulation the explicit evaluation of the incident potential, φ_I, is required only in the Bernoulli theorem that, in a body-fixed frame of reference, reads

$$\begin{aligned} \dot{\varphi}_S &+ \dot{\varphi}_I - \mathbf{v}_B \cdot (\nabla \varphi_S + \mathbf{v}_I) \\ &+ \frac{|\nabla \varphi_S + \mathbf{v}_I|^2}{2} + \frac{p}{\rho} = \frac{p_0}{\rho}. \end{aligned}$$

Here, the incident potential is obtained from integration of the incident velocity field by using the expression in Eq. (5) with thick-vortex modeling.

3. The Aeroacoustic Solver

The Ffowcs Williams and Hawkings (FWH) equation [6] has been proven to be the most efficient aeroacoustic prediction tool in aeronautics applications for subsonic and supersonic configurations. Here, it is applied to the analysis of helicopter rotors in BVI conditions.

Assuming that the fluid is compressible and undergoes transformations with negligible changes of entropy, for $f(\mathbf{x},t) = 0$ denoting a surface moving in the fluid and the bar some generalized differential operators, the FWH equation reads

$$\begin{aligned} c_0{}^2 \overline{\Box}^2 \tilde{\rho} &= \frac{\overline{\partial}}{\overline{\partial} t} \left[\rho_0 \, \mathbf{v}_B \cdot \nabla f \; \delta(f)\right] \\ &- \overline{\nabla} \cdot \left[\mathbf{P} \, \nabla f \; \delta(f)\right] \\ &+ \overline{\nabla} \cdot \left\{\overline{\nabla} \cdot \left[\mathbf{T} \; H(f)\right]\right\}, \; \forall \mathbf{x} \in \Re^3 \end{aligned} \tag{6}$$

where $\tilde{\rho} = \rho - \rho_0$ is the density perturbation field and $\overline{\Box}^2 = \dfrac{1}{c_0{}^2} \dfrac{\overline{\partial}^2}{\overline{\partial} t^2} - \overline{\nabla}^2$ denotes the generalized D'Alambert operator. In addition, $\mathbf{P} = (p - p_0)\,\mathbf{I} = \tilde{p}\,\mathbf{I}$ and $\mathbf{T} = \rho\,\mathbf{v} \otimes \mathbf{v} + (\tilde{p} - c_0{}^2 \tilde{\rho})\mathbf{I}$ denote the compressive stress tensor and the Lighthill tensor, respectively, $\mathbf{v}$ is the fluid velocity, whereas H and δ are the Heaviside and Dirac delta functions. The solution of the FWH equation can be achieved through a boundary integral representation. Observing that in the present analysis the non-linear terms are negligible, and following Refs. [12] and [13], the integral solution for the acoustic pressure disturbance, $p' = c_0^2 \tilde{\rho}$, is given as a combination of a linear thickness noise term, p'_T and a linear loading noise term, p'_L. Specifically, one obtains

$$p' = p'_T + p'_L \tag{7}$$

with

$$\begin{aligned} 4\pi p'_T(\mathbf{x},t) &= \int_{\mathcal{S}} \left[\frac{\rho_0 \dot{v}_{B\,n}}{r|1-M_r|^2}\right]_{\tau^*} \mathrm{d}\mathcal{S} \\ &+ \int_{\mathcal{S}} \left[\frac{\rho_0 v_{B\,n} \left(r\,\dot{\mathbf{M}} \cdot \hat{\mathbf{r}} + c_0 M_r - c_0 M^2\right)}{r^2 |1-M_r|^3}\right]_{\tau^*} \mathrm{d}\mathcal{S} \end{aligned} \tag{8}$$

and

$$\begin{aligned} 4\pi p'_L(\mathbf{x},t) &= \frac{1}{c_0} \int_{\mathcal{S}} \left[\frac{\left(\dot{\tilde{p}} \hat{\mathbf{r}} \cdot \mathbf{n} + \tilde{p}\,\dot{\mathbf{n}} \cdot \hat{\mathbf{r}}\right)}{r|1-M_r|^2}\right]_{\tau^*} \mathrm{d}\mathcal{S} \\ &+ \int_{\mathcal{S}} \left[\frac{\tilde{p} \hat{\mathbf{r}} \cdot \mathbf{n} - M_n}{r^2 |1-M_r|^2}\right]_{\tau^*} \mathrm{d}\mathcal{S} \\ &+ \frac{1}{c_0} \int_{\mathcal{S}} \left[\frac{\tilde{p} \hat{\mathbf{r}} \cdot \mathbf{n} \left(r \dot{\mathbf{M}} \cdot \hat{\mathbf{r}} + c_0 M_r - c_0 M^2\right)}{r^2 |1-M_r|^3}\right]_{\tau^*} \mathrm{d}\mathcal{S} \end{aligned} \tag{9}$$

where the symbol $\dot{(\;)}$ denotes time derivation, $\mathbf{r}$ denotes the distance between $\mathbf{x}$ and $\mathbf{y}$, $r = |\mathbf{r}|$, and $\hat{\mathbf{r}} = \mathbf{r}/r$. In Eqs. (8) and (9), the integration domain $\mathcal{S}$ denotes the surface of the *source*, which in the present analysis corresponds to the rotor blade surface, $\mathcal{S}_B$. In addition, $\mathbf{M} = \mathbf{v}_B / c_0$ is the local Mach vector, $M = |\mathbf{M}|$, $M_r = \mathbf{M} \cdot \hat{\mathbf{r}}$, and $M_n = \mathbf{M} \cdot \mathbf{n}$. This particular integral representation of the FWH linear terms is known as the Farassat Formulation 1A [12], and yields the acoustic field once the blade pressure disturbance distribution, $\tilde{p}$, is known from an aerodynamic analysis. Here, the blade pressure to be used in Eq. 9 is obtained from the formulation given in Section 2. The notation $[...]_{\tau^*}$ indicates that the kernel quantities must be evaluated at the emission time, τ^*. For given observer time, t, and location, $\mathbf{x}$, it represents the instant when the contribution to the noise signature was released from $\mathbf{y}$. The determination of τ^* is the *core* of the numerical algorithm and is achieved through an iterative procedure, as root of the following equation

$$\tau = t - \frac{r}{c_0} = t - \frac{|\mathbf{x} - \mathbf{y}(\boldsymbol{\eta}, \tau)|}{c_0} = \Phi(\tau)$$

where $\boldsymbol{\eta}$ is the position vector of source point in a frame of reference fixed with the body. Starting from the initial time, $\tau = t$, and the corresponding positive value, $f(\tau) = r/c_0$, the research for the root of the function $f(\tau) = [\tau - \Phi(\tau)]$ proceeds backwards, with a prescribed time step $\Delta\tau$, up to the first sign inversion; then, the emission time, τ^*, is captured by convergence of the iterative bisection method.

4. Numerical results

The aim of the numerical applications is to investigate the effect of the blade deformation on the aeroacoustic analysis of the four-bladed EC/ONERA 7A and 7AD main rotors in BVI conditions. The configurations examined are those considered at the DNW wind tunnel within the European Project HELISHAPE [14]. These two rotors, both having aspect ratio equal to 15, only differ by the shape of their tips. Specifically, rotor 7A has a rectangular tip whereas rotor 7AD has a parabolic tip with taper, anhedral and sweep angles. Both rotors are examined in 6°-descent forward flight condition, with rotational speed $\Omega = 101$rad/s and advance ratio

$\mu = 0.166$. The configurations analyzed are those related to the HELISHAPE Datapoint 70 for rotor 7A, and to the HELISHAPE Datapoint 108 for rotor 7AD.

In the following numerical investigation two models have been considered to describe the kinematics of the blade. The first one assumes that the blade is a rigid body subject to the cyclic pitch motion, whereas the second one includes also the elastic deformation that has been measured in the wind tunnel tests. The numerical analysis has been performed by assuming the azimuthal step $\Delta\psi = 1.33°$, and including a two-spiral long wake.

First, results concerning the blade pressure are presented. Figures 2 and 3 depict, respectively for rotors 7A and 7AD, the pressure time history on the profile upper and lower sides at the radial station $r = .92R$ and chordwise position $x = 0.02c$. These figures show a quite good agreement between the numerical results and the experimental data both in terms of detection of the regions where BVI occurs and in terms of the order of magnitude of the pressure oscillations induced by BVI. The solution obtained by the deformed blade is closer to the experimental data than that obtained by the rigid blade. This is especially true in the azimuthal regions in which BVI induces pressure oscillations. For the 7A and 7AD rotors these results demonstrate that the aerodynamic field in BVI conditions is appreciably dependent on the blade kinematics model included in the numerical computations. This fact is associated to the different relative positions between wake vortices and blade that occur in rigid-blade and deformed-blade analyses.

Then, the aeroacoustic fields obtained from the two blade models are presented. These have been obtained through the application of the formulation outlined in Section 3, using the blade pressure given by the aerodynamic formulation of Section 2. Figures 4-9 present the comparison between the measured acoustic pressure and the numerical acoustic time signature for both rigid and deformed blade model. Figures 4-6 concern rotor 7A, Figs. 7-9 concern rotor 7AD and these two groups of figures are related to the same observer positions. The observers are located 2.286m below the rotor disk. In the experimental tests, the first one (Obs A) corresponds to the upstream microphone 3 that is 2m distant from the rotor hub (advancing rotor side), the second one (Obs B) corresponds to the upstream microphone 3 located 3m far from the rotor hub (advancing rotor side), while the third one (Obs C) corresponds to the upstream microphone 9 located 3.5m far from the rotor hub (retreating rotor side). These figures show that the numerical results from the deformed-blade rotor are in good agreement with the experimental data, but the agreement between the experimental data and the numerical results from the rigid-blade rotor is quite poorer. Indeed, they demonstrate that using rigid blades, although the impulsiveness of the signal is captured, BVI peaks are underestimated, whereas the application of deformed blades yields results where the impulsiveness of the signal as well as the intensity of the peaks due to BVI are in good agreement with the wind tunnel measurements.

The overall quality of the numerical predictions can be assessed from Figs. 10-11. These concern the noise contour levels (expressed in dB) related to the arrays of microphones positioned on the horizontal plane located 2.286m below the rotor disk (these figures indicate also the positions on this plane of the three observers considered in Figs. 4-9). Results from experimental data and numerical analysis for rotor 7A are given in Fig. 10, whereas Fig. 11 is related to rotor 7AD. The observation of these figures confirms the good accuracy of the predictions given by the deformed-blade model both in terms of noise directivity and intensity of noise peaks. On the other hand, it is also confirmed that the predictions based on the rigid-blade model underestimate the intensity of the noise peaks produced by the BVI. They show also that the low-quality of the rigid-blade predictions concern the whole plane examined, with the poorest quality observed in the 7AD rotor analysis. Anyway, the rigid-blade analysis seems to correlate fairly well with the noise directivity pattern obtained from measurements.

Concluding remarks

An aeroacoustic prediction tool for helicopter rotors experiencing BVI has been presented. The aerodynamic solver is based upon a fully three-dimensional direct panel method that is suited for the analysis of helicopter rotors in BVI conditions, and which is applicable to arbitrarily shaped thick blade rotors in arbitrary flight mode. The numerical solver applied to evaluate the acoustic field is based on the Ffowcs Williams and Hawkings equation.

The results of the numerical investigation presented have been pointed to examine the sensitivity of the BVI noise predicted on the blade kinematic model included in the analysis. The analysis has been performed considering the EC/ONERA 7A and 7AD main rotors under rigid-blade and deformed-blade assumptions. The blade deflections measured in the wind tunnel tests have been used for the deformed-blade analysis.

The investigation shows that the numerical results including the blade deformation predict the BVI noise with a good level of accuracy both in terms of peak intensity and directivity. On the other hand, the numerical predictions using rigid blades, although capturing the noise peaks due to BVI, underestimate significantly their intensity. This occurs over the entire reagion considered and is especially true for the 7AD rotor. However, noise level contur plots have shown that the directivity of the acoustic signal is fairly well predicted by the rigid blade analysis.

Acknowledgments

This work has been partially supported by the European Union Integrated Project *Friendcopter* (Contract No. AIP3-CT-2003-502773).

References

1. Tung, C., Yu, Y.H., and Low, S.L., "Aerodynamic Aspects of Blade-Vortex Interaction (BVI)," AIAA Paper 96-2010, *Proceedings of the 27th AIAA Fluid Dynamics Conference*, New Orleans, LA, 1996.
2. Munsky, B., Gandhi, F., and Tauszig, L., "An Analysis of Helicopter Blade-Vortex Interaction Noise with Flight Path or Attitude Modification," *Proceedings of the 58th Annual Forum of the American Helicopter Society*, Montréal, Canada, 2002.
3. Liu, L., Patt, D., and Friedmann, P.P., "Simultaneous Vibration and Noise Reduction in Rotorcraft Using Aeroelastic Simulation," *Proceedings of the 60th Annual Forum of the American Helicopter Society*, Baltimore, MD, 2004.
4. Beaumier, P., and Delrieux, Y., "Description and Validation of the ONERA Computational Methods for the Prediction of Blade-Vortex Interaction Noise," *Aerospace Science and Technology*, Vol. 9, 2005, pp. 31-43.
5. Gennaretti, M., and Bernardini, G., "A Novel Potential-Flow Boundary Integral Formulation for Helicopter Rotors in BVI Conditions," AIAA Paper 2005-2924, *Proceedings of the 11th AIAA/CEAS Aeroacoustics Conference*, Monterey, California, May 2005.
6. Ffowcs Williams, J.E., and Hawkings, D.L., "Sound Generation by Turbulence and Surfaces in Arbitrary Motion," *Philosophical Transactions of the Royal Society*, Vol. A264, No. 1151, 1969, pp. 321-542.
7. Morino, L., "A General Theory of Unsteady Compressible Potential Aerodynamics," NASA CR-2464, 1974.
8. Morino, L., and Bharadvaj, B.K., "A Unified Approach for the Potential and Viscous Free-Wake Analysis of Helicopter Rotors," *Vertica*, Vol. 12, No. 1/2, 1988, pp. 147-154.
9. Morino, L., and Bernardini, G., "Singularities in Discretized BIE's for Laplace's Equation; Trailing-Edge Conditions in Aerodynamics," *Mathematical Aspects of Boundary Element Methods*, edited by M. Bonnet, A.M. Sändig, and W.L. Wendland, Chapman & Hall/CRC, London, UK, 2000, pp. 240-251.
10. Leishman, J.G., *Principles of Helicopter Aerodynamics*, Cambridge University Press, 2000.
11. Ananthan, S., Leishman, J.G., and Ramasamy, M., "The Role of Filament Stretching in the Free-Vortex Modeling of Rotor Wakes," *Proceedings of the 58th Annual Forum of the American Helicopter Society*, Montréal, Canada, 2002.
12. Farassat , F., "Linear Acoustic Formulas for Calculation of Rotating Blade Noise," *AIAA Journal*, Vol. 19, No. 9, 1981, pp. 1122-1130.
13. Farassat, F., and Brentner, K.S., "The Uses and Abuses of the Acoustic Analogy in Helicopter Rotor Noise Prediction," *Journal of the American Helicopter Society*, Vol. 33, No. 1, 1988, pp. 29-36.
14. Schultz K.J., Splettstoesser, W., Junker, B., Wagner, W., Schoell, E., Arnaud, G., Mercker. E., Pengel, K. and Fertis, D., "A Parametric Wind Tunnel Test on Rotorcraft Aerodynamics and Aeroacoustics (HELISHAPE) - Test Documentation and Representative Results," *Proceedings of the 22nd European Rotorcraft Forum*, Brighton, U.K., 1996.

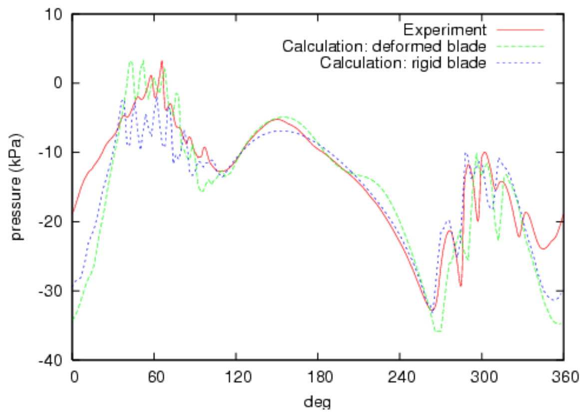

(a) Upper side

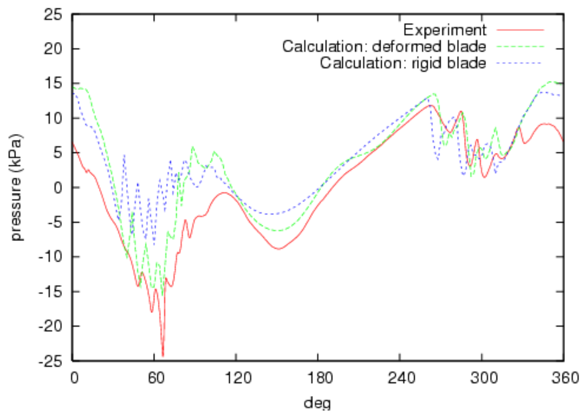

(b) Lower side

Figure 2. 7A rotor: time history of blade pressure at $r = .92R$, $x = 0.02c$

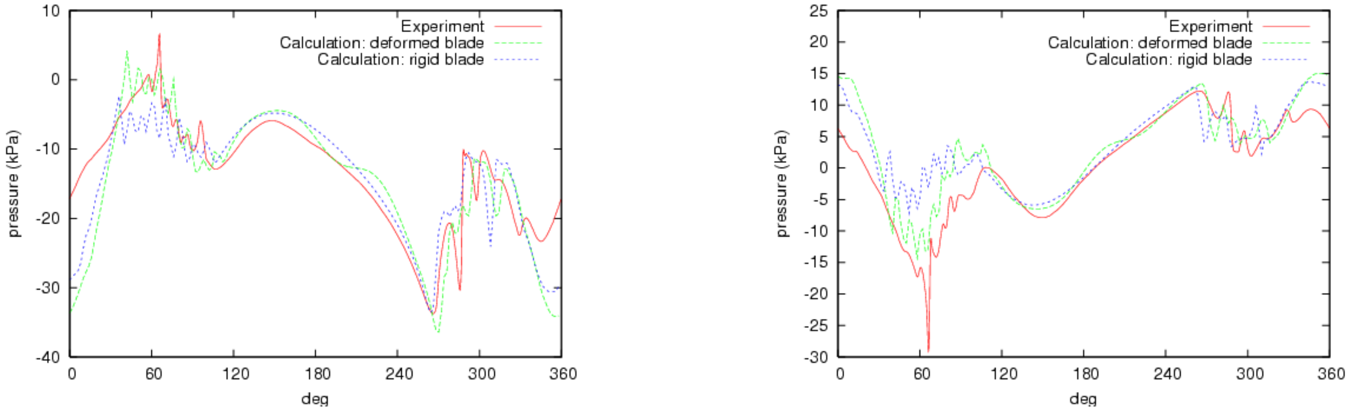

(a) Upper side

(b) Lower side

Figure 3. 7AD rotor: time history of blade pressure at $r = .92R$, $x = 0.02c$

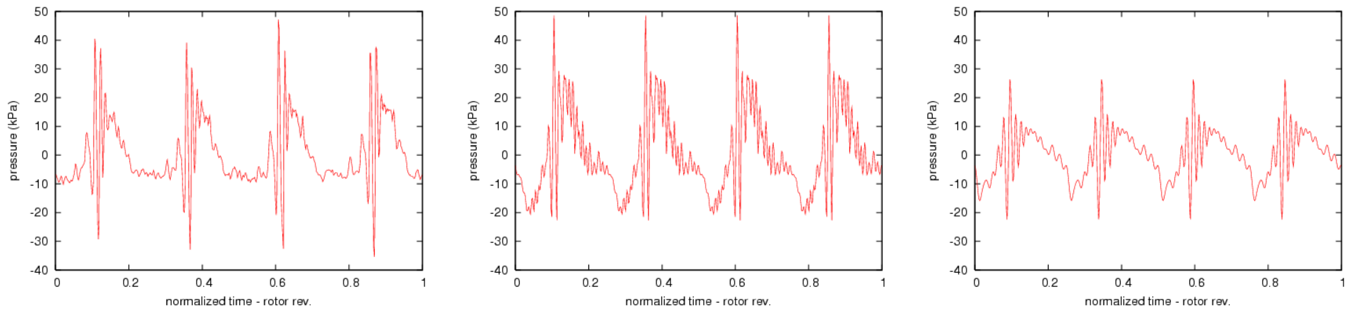

(a) Experiment

(b) Calculation: deformed blade

(c) Calculation: rigid blade

Figure 4. 7A rotor: acoustic signature at Obs A

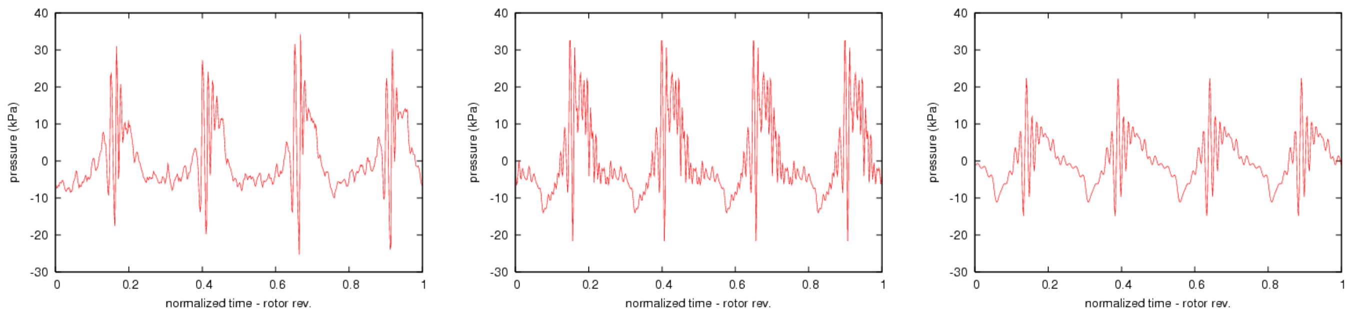

(a) Experiment

(b) Calculation: deformed blade

(c) Calculation: rigid blade

Figure 5. 7A rotor: acoustic signature at Obs B

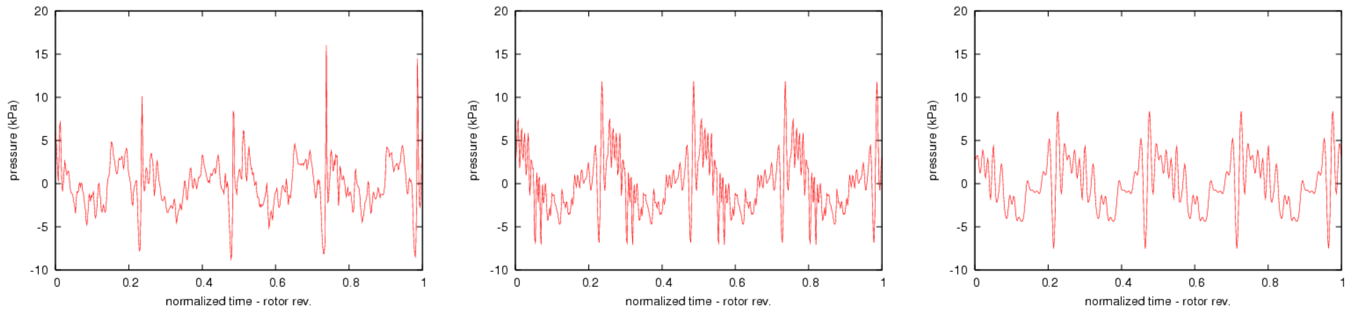

(a) Experiment (b) Calculation: deformed blade (c) Calculation: rigid blade

Figure 6. 7A rotor: acoustic signature at Obs C

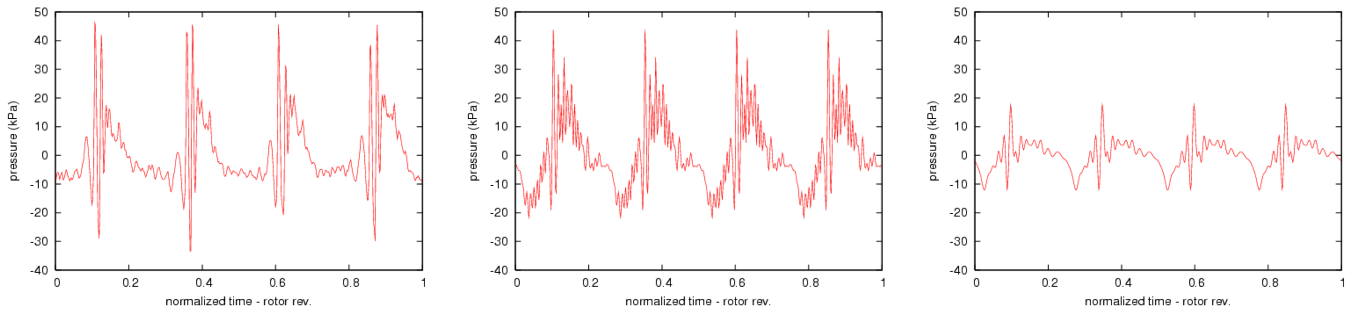

(a) Experiment (b) Calculation: deformed blade (c) Calculation: rigid blade

Figure 7. 7AD rotor: acoustic signature at Obs A

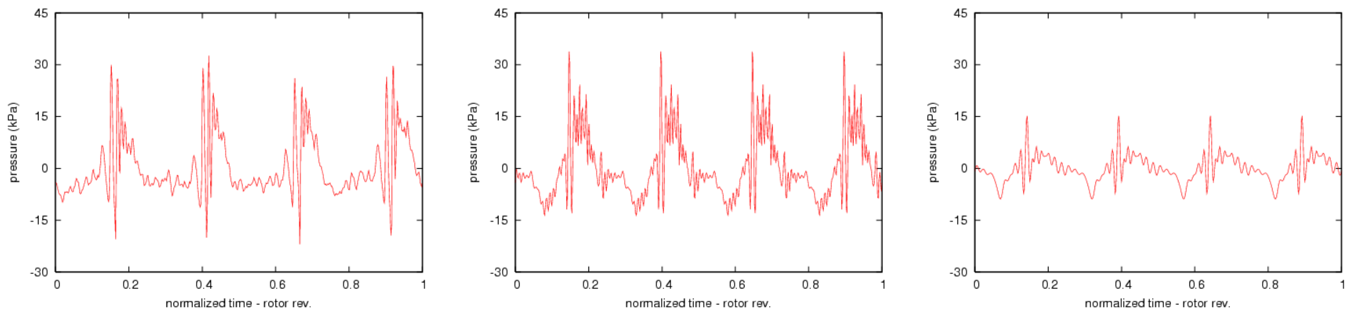

(a) Experiment (b) Calculation: deformed blade (c) Calculation: rigid blade

Figure 8. 7AD rotor: acoustic signature at Obs B

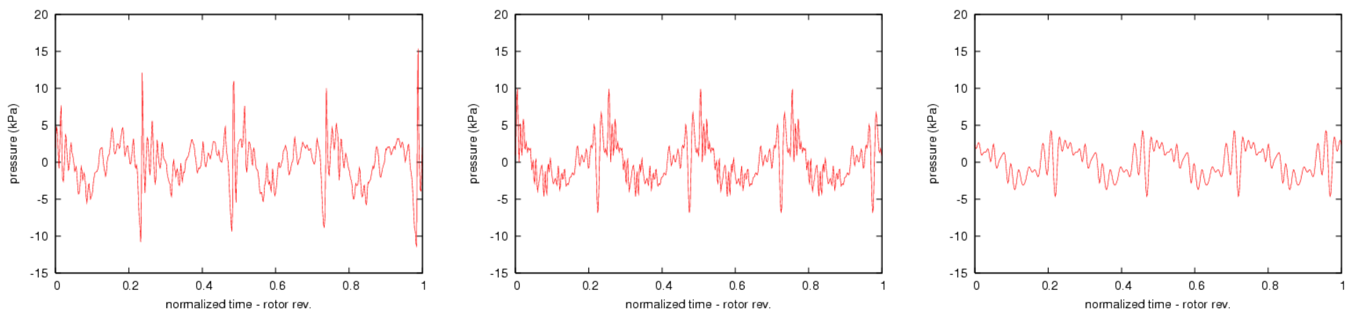

(a) Experiment (b) Calculation: deformed blade (c) Calculation: rigid blade

Figure 9. 7AD rotor: acoustic signature at Obs C

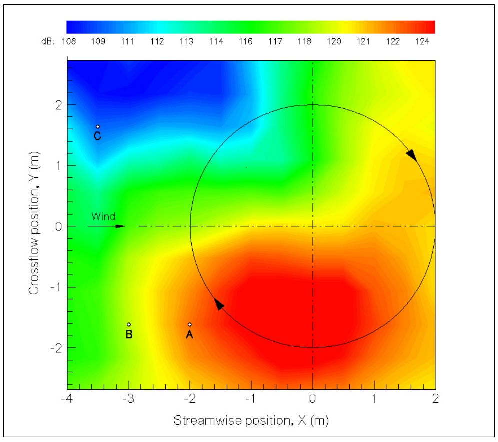

(a) Experiment

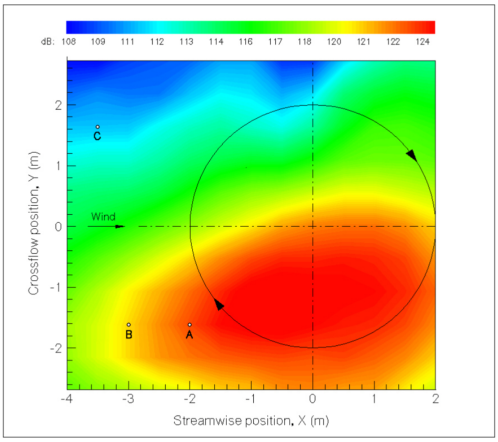

(b) Calculation: deformed blade

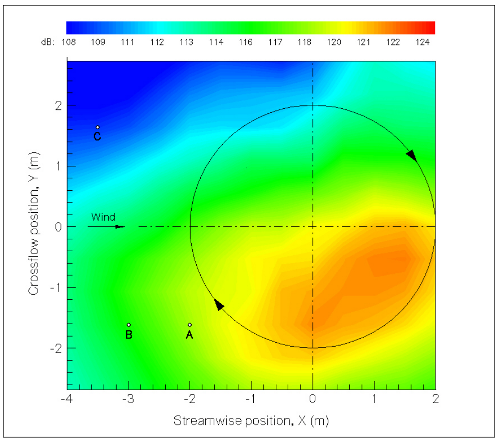

(c) Calculation: rigid blade

Figure 10. 7A rotor: noise contour levels

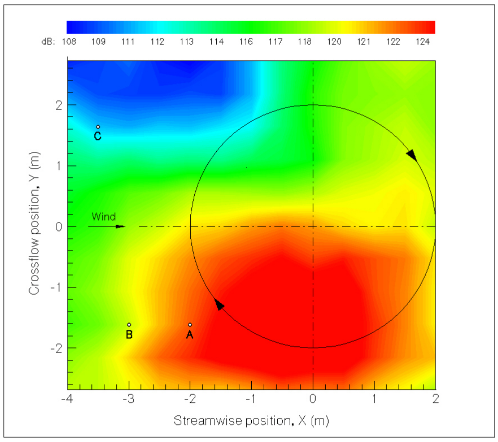

(a) Experiment

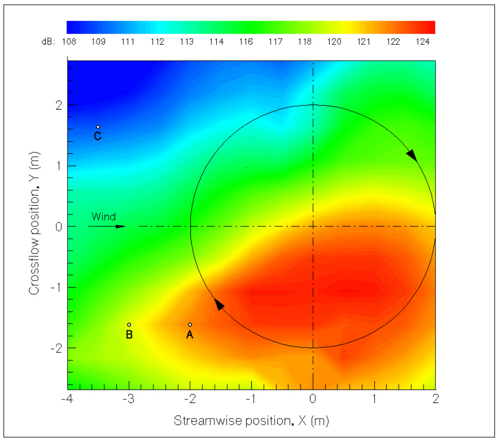

(b) Calculation: deformed blade

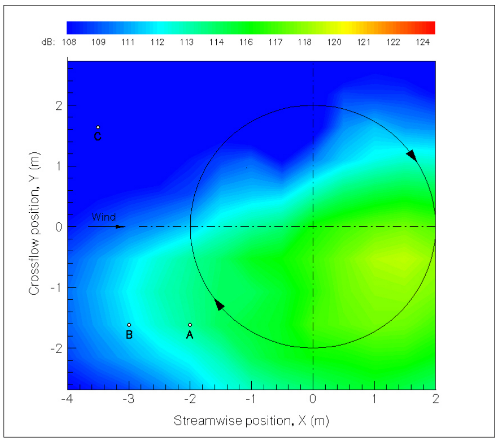

(c) Calculation: rigid blade

Figure 11. 7AD rotor: noise contour levels